Geophysical Journal International

Geophys. J. Int. (2014) **198,** 697–709
Advance Access publication 2014 June 2
GJI Mineral physics, rheology, heat flow and volcanology

doi: 10.1093/gji/ggu152

Simultaneous retrieval of volcanic sulphur dioxide and plume height from hyperspectral data using artificial neural networks

Alessandro Piscini,[1] Elisa Carboni,[2] Fabio Del Frate[3] and Roy Gordon Grainger[2]

[1] *Istituto Nazionale di Geofisica e Vulcanologia, Via di Vigna Murata,* 605 *Roma, Italy. E-mail: alessandro.piscini@ingv.it*
[2] *COMET, Atmospheric, Oceanic and Planetary Physics, University of Oxford, Parks Road, OX1* 3*PU Oxford, UK*
[3] *Earth Observation Laboratory, Engineering department Tor Vergata University, Via del Politecnico* 1, *I*-00133 *Rome, Italy*

Accepted 2014 April 24. Received 2014 April 23; in original form 2013 December 9

SUMMARY

Artificial neural networks (ANNs) are a valuable and well-established inversion technique for the estimation of geophysical parameters from satellite images; once trained, they help generate very fast results. Furthermore, satellite remote sensing is a very effective and safe way to monitor volcanic eruptions in order to safeguard the environment and the people affected by those natural hazards.

This paper describes an application of ANNs as an inverse model for the simultaneous estimation of columnar content and height of sulphur dioxide (SO_2) plumes from volcanic eruptions using hyperspectral data from remote sensing.

In this study two ANNs were implemented in order to emulate a retrieval model and to estimate the SO_2 columnar content and plume height. ANNs were trained using all infrared atmospheric sounding interferometer (IASI) channels between 1000–1200 and 1300–1410 cm^{-1} as inputs, and the corresponding values of SO_2 content and height of plume, obtained from the same IASI channels using the SO_2 retrieval scheme by Carboni *et al.*, as target outputs.

The retrieval is demonstrated for the eruption of the Eyjafjallajökull volcano (Iceland) for the months of 2010 April and May and for the Grimsvotn eruption during 2011 May.

Both neural networks were trained with a time series consisting of 58 hyperspectral eruption images collected between 2010 April 14 and May 14 and 16 images from 2011 May 22 to 26, and were validated on three independent data sets of images of the Eyjafjallajökull eruption, one in April and the other two in May, and on three independent data sets of the Grímsvötn volcanic eruption that occurred in 2011 May. The root mean square error (RMSE) values between neural network outputs and targets were lower than 20 Dobson units (DU) for SO_2 total column and 200 millibar (mb) for plume height.

The RMSE was lower than the standard deviation of targets for the Grímsvötn eruption. The neural network had a lower retrieval accuracy when the target value was outside the values used during the training phase.

Key words: Image processing; Neural networks, fuzzy logic; Inverse theory; Volcanic gases; Remote sensing of volcanoes; Volcano monitoring.

1 INTRODUCTION

The eruption of the Eyjafjallajökull volcano, which took place in Iceland in 2010 April and May, revealed the importance of monitoring volcanic eruptions for human safety (Zehner 2010) and showed the value of having reliable real-time monitoring in place for volcanic ash and sulphur dioxide (SO_2), especially for the aviation sector (Miller & Casadevall 2000). Volcanic ash plumes from the eruption of Eyjafjallajökull in April 2010 resulted in the cancellation of 107 000 flights in Europe (or 48 per cent of total traffic) affecting about 10 million passengers.

Estimating SO_2 is a very important task because of the critical role that its plume plays as a proxy for volcanic ash, especially within a few hours after release when the effects of wind shear and of gravitation have not yet divided the ash plume from the SO_2 (Thomas & Prata 2011). For these reasons, accurate and readily available data are needed to properly monitor the evolution of the phenomena and to manage the risk mitigation phase.

Estimates of SO_2 by satellite are performed using multispectral data from various sensors such as the MODerate resolution imager Spectroradiometer (MODIS; Watson *et al.* 2004; Corradini *et al.* 2008), the Advanced Spaceborne Thermal Emission and Reflection

Radiometer (ASTER; Urai 2004; Campion *et al.* 2010) and the Spinning Enhanced Visible and Infrared Imager (SEVIRI; Realmuto *et al.* 1997; Watson *et al.* 2004; Pugnaghi *et al.* 2006; Prata & Kerkmann 2007; Corradini *et al.* 2009, 2010).

Quantitative estimation of SO_2 is usually obtained by applying algorithms based on a comparison between top of atmosphere radiance and values obtained from simulations run using a radiative transfer (RT) model: this requires long computation times and many parameters as input (Berk *et al.* 1989; Anderson *et al.* 1995). Recently, efforts to increment the speed of computation in SO_2 retrieval procedures have been carried out using a customized version of MODerate resolution atmospheric TRANsmission (MODTRAN) RT model under a single user interface (Realmuto *et al.* 2013).

More recent estimates of columnar content of SO_2 in the atmosphere as a result of volcanic eruptions are available using hyperspectral data from various sensors operating in different spectral ranges from ultraviolet (UV) to thermal infrared (TIR).

The use of the spectral information allows retrieval of the SO_2 amount, generally by assuming the altitude of the plume (Clarisse *et al.* 2012). Recently both UV and TIR spectra have also been exploited to retrieve information on altitude of the plume (Clerbaux *et al.* 2008; Yang *et al.* 2009; Clarisse *et al.* 2014). The Global Ozone Monitoring Experiment (GOME-2), on-board Meteorological Operational (MetOp-A) satellite, is a UV spectrometer that measures SO_2 in the UV absorption band and has been used for optimal estimation (OE) retrievals of SO_2 (Nowlan *et al.* 2011; Rix *et al.* 2012). Aura Ozone Monitoring Instrument (OMI) is a UV spectrometer and has been used for the retrieval of SO_2 using a 'band residual difference' algorithm (Krotkov *et al.* 2006).

Satellite infrared spectrometers, such as atmospheric infrared sounder (AIRS) and the tropospheric emission spectrometer (TES), or IASI, can measure volcanic SO_2 in three spectral regions; around 4.0, 7.3 and 8.7 μm (called, respectively, the $\nu_1 + \nu_3$, ν_3 and ν_1 absorption bands). The 4.0 μm absorption feature ($\nu_1 + \nu_3$) is weak, and reflected solar radiation is significant during daytime. The 7.3 μm feature (ν_3 band) is the strongest of the three bands. It is collocated with a strong water vapour absorption band and, as a consequence, it contains information on the SO_2 vertical profile, but it is less sensitive to the lower tropospheric layers. IASI measurements in this band have been used in OE retrievals (Clarisse *et al.* 2008), in a fast SO_2 retrieval with an assumed plume altitude (Clarisse *et al.* 2012) and recently in a fast algorithm that estimates the SO_2 altitude (Clarisse *et al.* 2014).

The 7.3 μm feature has been used to retrieve SO_2 amount from AIRS data (Carn *et al.* 2005; Prata & Bernardo 2007) with an assumed plume altitude. The 8.7 μm absorption feature (ν_1 band) also contains information on the SO_2 amount for lower tropospheric plumes and has been used to retrieve the total SO_2 amount and profile from TES data (Clerbaux *et al.* 2008). At the IASI spectral resolution (lower then TES) this region alone does not contain information to retrieve the SO_2 profile but it is probably the most useful region for monitoring those volcanoes characterized by continuous quiescent degassing (Realmuto *et al.* 1997; Realmuto 2000).

Carboni *et al.* (2102) used an OE scheme for retrieving SO_2 amount and plume height from nadir IASI thermal infrared measurements of the ν_3 and ν_1 absorption bands.

Fig. 1 shows a comparison between estimates from the different sensors described above for the 2010 Eyjafjallajökull eruption. It is noticeable that during some phases of eruption the retrievals obtained using TIR or UV bands are consistent, while at other times the mass estimates disagree. There is a need for comparison of results obtained using different retrieval schemes and instruments

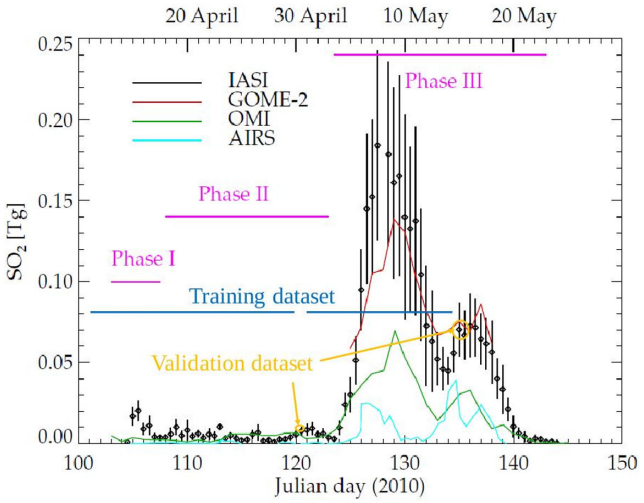

Figure 1. Total mass of SO_2 present in the Eyjafjallajökull plume: IASI data (and error bars) are shown in black (Carboni *et al.* 2012), GOME-2 values (Rix *et al.* 2012) are shown in red, OMI values (Thomas & Prata 2011) are shown in green, AIRS values (Thomas & Prata 2011) are shown in cyan. Training and validation periods are indicated with dark blue and yellow.

in order to better understand the retrieval results and to identify problematic conditions. This work focuses mainly on testing the ability of the neural network to reproduce the results of the OE scheme. The validation of the OE algorithm and the comparison of the results with other algorithms and data sets was outside the scope of this study.

ANNs represent computational modelling tools that have found wide acceptance in many disciplines due to their adaptability to complex real world problems. They have demonstrated their ability to model non-linear physical systems (Rumelhart *et al.* 1995) involving complex behaviours, taking into account any non-linear relationships between the explanatory and dependent variables (Lek & Guegan 1999). Such a technique does not need the ancillary data necessary to the algorithms used for parameter retrieval, and once the training phase is completed, it can be applied to different independent data sets in near real time. Some examples of the use of ANNs applied to atmospheric remote sensing for inverse modelling are: retrieval of cloud parameters from high-resolution multispectral data (Faure *et al.* 2002), retrievals of ozone profiles in the atmosphere (Del Frate *et al.* 2002), retrieval of temperature and moisture profiles from high spectral resolution sounding data (Blackwell 2005), retrieval of atmospheric water vapour and cloud liquid water (Vasudevan *et al.* 2004), retrieval of volcanic ash mass from multispectral data (Picchiani *et al.* 2011).

Recently, ANNs have been applied to MODIS multispectral measurements to retrieve volcanic ash parameters such as ash mass, effective radius, aerosol optical depth and SO_2 columnar content (Piscini *et al.* 2014), and ANNs have also been used operationally to estimate CO, CO_2 and CH_4 column amounts from IASI (Schlüssel *et al.* 2005). This study represents a first attempt at applying ANNs to hyperspectral remote sensing data, emulating an inverse model for estimates of SO_2 total columnar content and the plume height. This work, compared to recent results of ANNs usage with multispectral data, shows significant added value in reduced execution times during the application stage.

The following section describes characteristics of IASI hyperspectral sensors, as well as the algorithms applied to the data used to estimate columnar content of SO_2 and plume height. In Section 3,

the methods used for the development and learning phases of the network are described. In Section 4, the eruptions of Eyjafjallajökull and Grímsvötn volcanoes are described. In Section 5, some preliminary results of neural network application to independent data sets are reported and discussed. Finally, Section 6 completes the work with conclusions and future perspectives.

2 DATA: MEASUREMENTS AND RETRIEVALS

2.1 MetOp-IASI sensor

The IASI sensor is aboard MetOp, a European weather satellite which has been operating since 2007. MetOp is the first of three satellites scheduled to operate for 14 yr. Its orbit crosses the Equator with a descending node local time of 9.30. IASI is a Fourier transform spectrometer which covers the spectral range 645–2760 cm^{-1} (3.62–15.5 μm) with spectral sampling of 0.25 cm^{-1} and apodized spectral resolution of 0.5 cm^{-1} (Blumstein *et al.* 2004). It has a nominal radiometric accuracy of 0.25–0.58 K. The field-of-view (FOV) consists of four circular footprints of 12 km diameter (at nadir) inside a square of 50 × 50 km, step-scanned across tracks (30 steps). It has a 2000 km wide swath and nominally it can achieve global coverage in 12 hr. Observations are collocated with the advanced very high resolution radiometer (AVHRR), providing complementary visible/near infrared measurements. IASI carries out nadir observation of the Earth simultaneously with Global Ozone Monitoring Experiment (GOME-2) also onboard MetOp. GOME-2 is a UV spectrometer measuring SO_2 in the UV absorption band and was used for both differential optical absorption spectroscopy (DOAS; Rix *et al.* 2012) and OE retrievals of SO_2 (Nowlan *et al.* 2011); more information on IASI can be found in Clerbaux *et al.* (2009).

The IASI level 1c data (geolocated and apodized spectra) used here were obtained from both the British Atmospheric Data Centre (BADC) archive and EUMETSAT Unified Meteorological Archive Facility (UMARF) archive.

IASI can retrieve SO_2 down to the surface, but note that the error associated with both the retrieved amount and altitude increases with decreasing altitude (see Carboni *et al.* 2012 for more detail on error analysis). In particular, the algorithm is especially designed for middle/small eruptions and makes use of both the ν_1 absorption band around 8.7 μm (in the atmospheric windows range) as well as the ν_3 absorption band around 7.3 μm (within the water vapour absorption band). The spectral region around the ν_1 band has been included in order to have the maximum of information down to the surface. Nevertheless Boynard *et al.* (2014) recently demonstrated IASI has the capability, using only the ν_3 absorption band, to retrieve SO_2 from anthropogenic pollution.

2.2 SO_2 total column content and plume height retrieval description

Values used here were obtained with the OE scheme to retrieve SO_2 column amount and altitude from nadir satellite TIR measurements using the two SO_2 absorption bands centred at about 8.7 and 7.3 μm, the ν_1 and ν_3 bands, respectively; more details of the retrieval are in Carboni *et al.* (2012). This retrieval technique uses an error covariance matrix, $\mathbf{S}_e$, based on an SO_2-free climatology of differences between the IASI measurements and forward modelled spectra. Any differences not related to SO_2 between IASI spectra and those simulated by a forward model are included in the covariance matrix, allowing a comprehensive error budget to be computed for every pixel.

As IASI measures atmospheric emission, it provides continuous measurements throughout an orbit. The IASI retrieval follows the method of Carboni *et al.* (2012) where SO_2 concentration is modelled by a Gaussian profile. The OE technique of Rodgers (2000) is then used to estimate SO_2 column amount and the height of the SO_2 profile, and the surface skin temperature using IASI measurements from 1000 to 1200 cm^{-1} and from 1300 to 1410 cm^{-1} (the ν_1 and ν_3 SO_2 bands). Retrieval is performed minimizing a cost function J defined as:

$$J = (\mathbf{y} - \mathbf{F}(\mathbf{x}, \mathbf{b}) - c)^T \mathbf{S}_e^{-1} (\mathbf{y} - \mathbf{F}(\mathbf{x}, \mathbf{b}) - c) + (\mathbf{x} - \mathbf{x}_a)^T \mathbf{S}_a^{-1} (\mathbf{x} - \mathbf{x}_a),$$

where **F(x,b)** is the forward model (i.e. the function which maps state parameters to measurements), **x** is a vector of retrieved values, **b** are other parameters in the forward model (as for example temperature and water vapour profile), **y** the measurement vector, $\mathbf{S}_e$ is the measurement error covariance matrix, $\mathbf{x}_a$ is the *a priori* state vector, $\mathbf{S}_a$ is the *a priori* error covariance matrix and c is a bias term that represents the mean difference between the measurements **y** and the simulated spectra **F(x,b)** derived from SO_2 free scenes.

The forward model is based on RT for TOVS (RTTOV; Saunders *et al.* 1999), extended to include SO_2 explicitly, and uses European Centre for Medium-Range Weather Forecasts (ECMWF) profiles of temperatures and water vapour interpolated to the time and location of the IASI measurement. The ECMWF data set used is the operational one: http://www.badc.rl.ac.uk/data/ecmwf-op/.

Note that: (i) in addition to the SO_2 column amount, retrievals return an estimate of the plume altitude (under the assumption that vertical concentrations of SO_2 follow a Gaussian distribution) when the column amount is $>\sim$2 Dobson units (DU) and the plume height represents the altitude where the Gaussian profile reaches a maximum; (ii) SO_2 retrieval is not affected by underlying clouds (if SO_2 is within or below an ash or cloud layer its signal will be masked and retrieval will underestimate the SO_2 amount; in the case of ash this is indicated by a cost function value greater than two); (iii) an error covariance matrix is provided per pixel.

Retrieval includes a comprehensive error budget for every pixel derived from an error covariance matrix based on an SO_2-free climatology of the differences between IASI measurements and forward modelled spectra.

Rigorous error propagation, including the incorporation of forward model and forward model parameter error, is built into the system, providing quality control and error estimates on the retrieved state.

The main contribution to the error budget arises from assumptions of plume shape. Secondary contributions come from uncertainty in atmospheric parameters such as the temperature profile.

In the case of two or more plume layers the assumption of one layer (Gaussian vertical profile) could be a source of error on the retrieved altitude (and this error is not included in the pixel-by-pixel error estimate).

The altitude of the SO_2 plume strongly modulates the retrieval error, as the contrast between plume temperature and surface temperature is a critical factor. The error in SO_2 amount decreases with an increase in plume altitude. Typical uncertainties are 2 DU for a plume centred at 1.5 km and $<$1 DU for plumes above 3 km. More details of the retrieval are in Carboni *et al.* (2012).

The total mass of SO_2 in the atmospheric plume is obtained by interpolating the accepted data into a 0.125° grid. In particular,

every interpolated grid-box column amount is multiplied by the grid-box area to obtain the SO_2 mass, and all the grid-boxes masses are summed together to obtain the total mass of SO_2 for every IASI image. The time series of these total masses is presented in Fig. 1.

Error bars shown are the worst scenario of correlated error, obtained as a sum of all pixel errors (an overestimate, compared to independent errors). Fig. 1 shows the values of total mass obtained considering all the plume pixels (with latitude between 30°N and 80°N and longitude between −50° and 40°E), taking into account only the pixels complying with quality control criteria (convergence and cost function lower than two). Results show that the SO_2 retrieval scheme for IASI follows the different phases of a medium intensity eruption in the lower troposphere such as Eyjafjallajökull, in some phases consistent with GOME-2, OMI, even if estimates from different satellites can vary significantly.

3 NEURAL NETWORKS METHODOLOGY

This work uses a Backpropagation Artificial Neural Network (BPANN). Such networks are widely used for their flexibility and adaptability in modelling a wide spectrum of problems in many application areas (Rumelhart *et al.* 1986). Moreover, in Gardner & Dorling (1998) and in Hsieh & Tang (1998) it was shown how this kind of ANNs can be highly effective in the solution of atmospheric inverse problems.

A BPANN is a Multi-Layer Perceptron (MLP) consisting of an input layer with nodes representing input variables to the problem, an output layer with nodes representing the dependent variables (i.e. what is being modelled), and one or more hidden layers containing nodes to help capture non-linearities in the data, in which the neurons can be fully or partially interconnected (Hecht-Nielsen 1990). Using supervised learning, with the error-correction learning rule for network weights adjustment, those networks can learn to map from one data space to another using examples (Rumelhart *et al.* 1986; Bishop 1995; Haykin 1999). Networks like this are versatile and can be used for data modelling, classification, forecasting, control, data and image compression, as well as pattern recognition (Hassoun 1995).

The performance of a trained ANN is generally assessed by computing the root mean squared error (RMSE) between expected values and activation values at the output nodes.

An ANN for SO_2 total column estimation and another for SO_2 plume height estimation were implemented using, as training sets, SO_2 column content values and SO_2 plume height values from IASI OE retrieval (Carboni *et al.* 2012), computed processing brightness temperatures from 58 IASI images of the Eyjafjallajökull eruption and 16 IASI images from the Grímsvötn eruption. Data were acquired from both morning and afternoon orbits in the periods 2010 April 14 to May 15 and 2011 May 16 to May 22. Both networks used acquired brightness temperature data as neural network inputs and SO_2 total column and plume height as target outputs, respectively. Sample patterns of statistics encompassed the duration of the Eyjafjallajökull eruption and partially for Grímsvötn, and they were considered a good training ensemble because data covered all three eruptive phases of the Eyjafjallajökull eruption. Spatial and statistical distributions of training sets for SO_2 columnar content and plume height are shown in Fig. 2, top-left and top-right. Network topologies, both for SO_2 total column content and plume height neural network, consisted of 1242 inputs, all IASI channels, representing the range of wavelengths which contain information on SO_2 and used in the IASI retrieval, 10 neurons in one hidden layer and one output.

When training a neural network, users aim at achieving optimal performance in terms of generalization. Generalization performance means small errors on examples not encountered during training (the so-called validation data set). A drawback of standard neural networks, which have almost always too large a parameter space, is a trend to overfitting. This means that error on unseen examples begins to increase (Geman *et al.* 1992). Cross-validation can be used to detect when overfitting starts during supervised training of a neural network (early stopping); training is then stopped before convergence to avoid overfitting. Early stopping using cross validation was done by splitting the training data into a training set, a test set, and a validation set, and then training the networks using only the training set, and evaluating the per-example error on the test set on a sample basis after a defined number of epochs. Finally, training was stopped when the error, the difference between neural network output and target (retrievals from Carboni *et al.* 2012), on the test set was higher than the previous error value (Prechelt 1998).

Percentages chosen were 70, 20 and 10 per cent of samples as training, test and validation sets, respectively. The last represented a validation-independent set utilized to test the networks' performance at the end of the early stopping procedure. Three IASI images for the Eyjafjallajökull eruption of 2010 April 30, afternoon orbit, and 2010 May 15, both morning and afternoon orbits, and three IASI images for the Grímsvötn eruption, 2011 May 22, 23 and 24, were used as independent sets for the ANN performance validation.

In most function approximation problems a single hidden layer is sufficient to approximate continuous functions (Hecht-Nielsen 1990; Basheer 2000). However, two hidden layers may be necessary for learning functions with discontinuities (Masters 1994). Determination of the appropriate number of hidden layers and number of hidden nodes in each layer is one of the most critical tasks in ANN design. Unlike the input and output layers, one starts with no prior knowledge as to the number and size of hidden layers. With an increasing number of hidden nodes, training becomes overly time-consuming.

The approach used to find an optimal number of hidden nodes was heuristic: to start from the maximum value of hidden nodes given by the a known algorithm (Masters 1994) and to train the network, then estimating accuracy. The next step consisted of subtracting one hidden node, and then retraining the network again, evaluating the accuracy. We stopped the procedure of hidden nodes subtraction when the accuracy started to get worse.

4 TEST CASES DESCRIPTION: THE EYJAFJALLAJÖKULL ERUPTION IN 2010 APRIL AND MAY. THE GRÍMSVÖTN ERUPTION IN 2011 MAY

4.1 Eyjafjallajökull

Eyjafjallajökull is one of Iceland's smaller ice caps, situated in the far south. It is located to the north of Skógar and to the west of the larger Mýrdalsjökull ice cap.

It covers the caldera of a volcano 1666 m high, which has erupted relatively frequently since the last ice age. The most recent major eruptions occurred in 1921, 1612 and from 1821 to 1823 (Global Volcanism Program 2013). The first phase of the recent eruption lasted from 2010 March 20 to April 12 and was characterized by

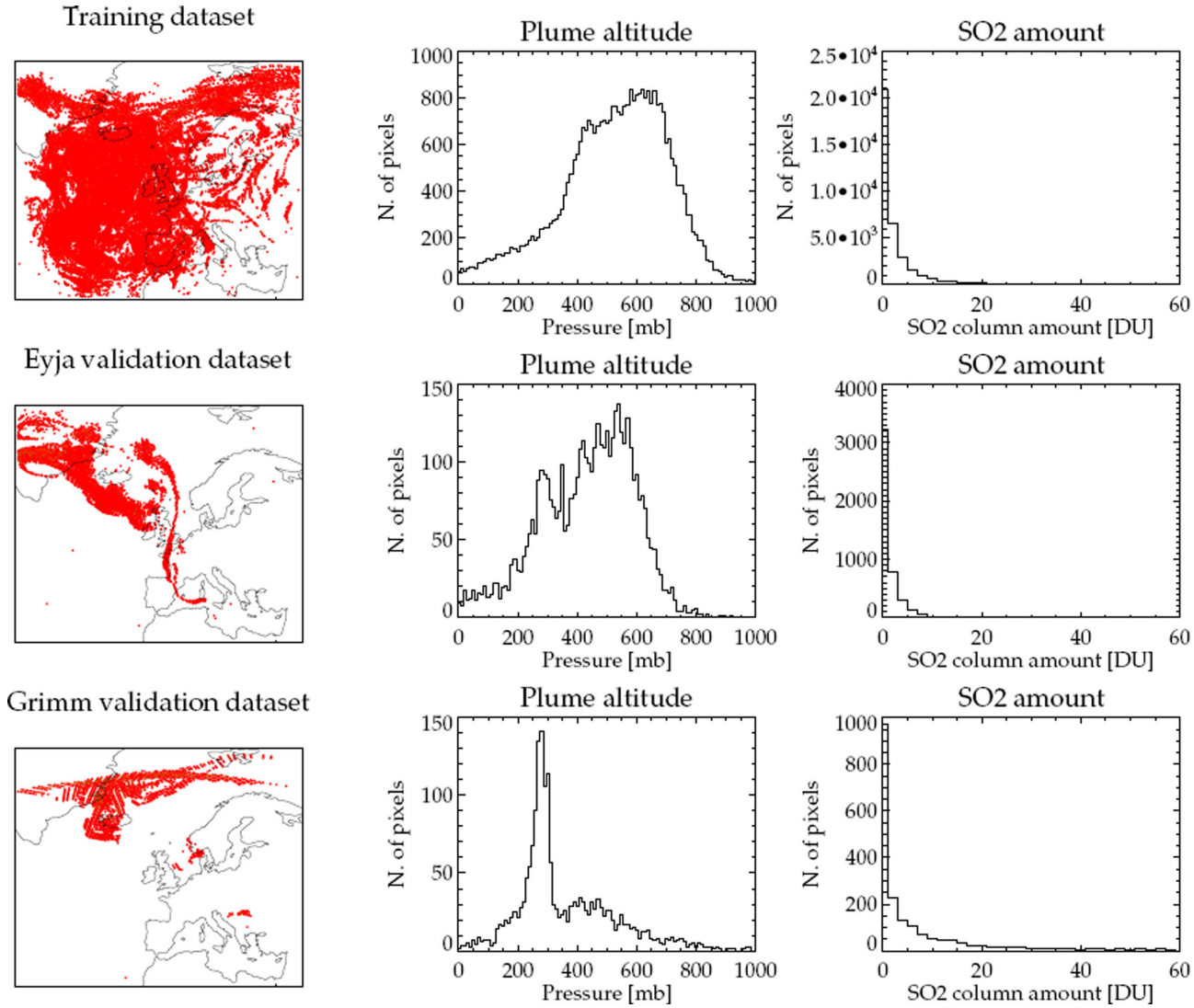

Figure 2. Spatial distribution maps of IASI SO_2 (left-hand panels), divided into training set (top panels), Eyjafjallajökull validation data set (middle panels), Grímsvötn validation data set (bottom panels) and histograms of SO_2 plume height and total column amount for each data set (middle and right-hand panels).

alkali-olivine basalt lava flowing from various eruptive vents on the flanks of the mountain and no significant ash or SO_2 emission. After a short hiatus in eruptive activity, a new set of craters opened early in the morning of 2010 April 14 under the ice-covered central summit caldera, anticipated by a series of earthquakes in the night between 13 and 14 April, and an explosive eruptive phase of the Eyjafjallajökull volcano began during the day. The explosive part of the eruption was divided into three phases (Zehner 2010).

Phase I: April 14–18

A phreatomagmatic eruptive phase: melt-water started to emanate from the ice cap around 07:00 on 14 April and an eruption plume was observed in the early morning. An ash-loaded eruption plume rose up to more than 8 km, deflected to the east by westerly winds (Marzano *et al.* 2011; Stohl *et al.* 2011).

Phase II: April 18–May 4

The eruption continued, but less explosively, with the plume rising to 5 km with a substantial reduction of ash transported into the atmosphere (Zehner 2010; Stohl *et al.* 2011). The eruption plume extended to altitudes between 4 and 5.4 km and was visible as far as 200 km from the eruption site. The wind direction on 2010 May 3 was pushing the ash cloud in a southeasterly direction, towards Britain.

Phase III: 5–24 May

Several earthquakes were detected beneath Eyjafjallajökull at 14–20 km depth. More explosive activity and ash production were reported than was observed during the previous day. The majority of the ash cloud rose up to 6 km, with some parts rising up to a maximum of 9 km. Unstable air from the south affected the height of the ash cloud, which headed in a southeasterly direction (Stohl *et al.* 2011). During this period, plumes of ash were transported to Europe and to the Atlantic Ocean.

The SO_2 volcanic plume could be tracked by IASI, as presented by Walker *et al.* (2011, 2012), choosing a statistical criteria for false detection. In their analysis, a threshold to define the volcanic plume was fixed to 1 over 10 000, meaning, with a high degree of confidence, one false detection (a pixel without any volcanic SO_2

Table 1. Eyjafjallajökull. RMSE and mean percentage difference between the ANN SO_2 total column amount and reference retrievals (Carboni *et al.* 2012). Also given are the STD of reference retrievals.

Date	SO_2 total column				
	N samples	Regr. coeff.	RMSE (DU)	STD (DU)	Mean diff. per cent
2010 April 30 aft	161	0.9523	0.7577	1.8084	16.9529
2010 May 15 mor	1823	0.93008	1.0523	2.7471	4.3728
2010 May 15 aft	2303	0.94372	0.8722	2.1335	8.7850

detected as volcanic plume) every ten thousand pixels. All IASI pixels detected as 'volcanic plume' were analysed with the SO_2 retrieval procedure.

IASI is able to follow the SO_2 volcanic plume with an image, composed from multiple orbits, acquired every half day.

4.2 Grímsvötn

Grímsvötn is a subglacial volcano, located 140 km NE of the Eyjafjallajökull volcano, in the western region of the glacier Vatnajökull, the largest in Europe. On 2011 May 21, Grímsvötn began to erupt, producing plumes of ash dispersed towards the western areas of Norway, Denmark and other parts of Northern Europe, with serious adverse consequences for air traffic. It was the first volcanic eruption since 2004, with ash dispersed as far as Finland; it stayed active from the 2011 May 21 to 28.

The eruption began in the late afternoon of 2011 May 21. According to the Icelandic Meteorological Office, the plume was monitored by two radars, one located at the Keflavík International Airport, more than 220 km away from the volcano, and a mobile radar, about 80 km away from the volcano. The height reached by the plume on the evening of May 21 was 20 km and it decreased to 15 km during the night. A few hours after the eruption began, ash-fall covered an area south of the Vatnajökull ice cap, more than 50 km away from the eruption site. During May 22–23, the ash plume rose to an altitude of 5–10 km and drifted south at lower altitudes, and west at altitudes of 8 km and higher. Ash-fall was detected in several areas throughout Iceland, with the exception of some areas in the NW (Global Volcanism Program 2013).

5 RESULTS AND DISCUSSION

The generalization capability and retrieval accuracy of neural networks was evaluated for three distinct independent IASI images of the Eyjafjallajökull eruption (see Section 4.1), and to three independent data sets related of the Grímsvötn volcanic eruption which occurred during May 2011 (see Section 4.2). The Eyjafjallajökull validation data set included an image from the morning and afternoon orbit of the same day (2010 May 15) in order to verify neural network performance in different illumination conditions. The third image (April 30) was chosen to test the ANN performance for low SO_2 concentrations. Fig. 2 shows the spatial distribution of the total mass of SO_2 for the Eyjafjallajökull training and validation data sets. These images were not considered during the training phase.

Table 1 summarizes the error statistics of the neural network technique applied to the three validation images, comparing total column SO_2 from the ANNs with retrievals obtained by Carboni *et al.* (2012). It show RMSE, standard deviation (STD) of target samples and difference percentage of ANN mean estimated value versus mean value of target.

The total column SO_2 RMSE is, for all three data sets, lower than the corresponding values of the targets' STD. In particular, looking at Table 1, we can see that the 30 April validation shows the lowest RMSE value and the highest regression coefficient, see Fig. 3 (top left).

An interesting behaviour of the ANN is seen in the May results. The regression coefficient is always around 0.9 (0.93 for morning orbit and 0.94 for afternoon orbit) but looking at the regression curves depicted in Fig. 3, middle-left and bottom-left, respectively, there is a decrease of accuracy for target values higher than 10 DU. This loss of accuracy increases for values higher than 20 DU.

We hypothesised that the better performance of the ANN in April is due to a lower number of samples (one order of magnitude with respect to the other two dates) and a range of values always below 10 DU, which represent 92.5 per cent of the training sample values. Nevertheless, considering the difference percentage of estimate and target means (Table 1, last column) the April results show an overestimate of retrievals with higher percentage. The good performance of the ANN for SO_2 retrieving is confirmed by Figs 4 and 5 (top) representing the comparison of the ANN retrieval map with those from Carboni *et al.* (2012).

Statistical results of applying the neural network to plume height estimation are summarized in Table 2. It is noticeable that for all three data sets RMSE is always below the corresponding values of the targets' STD. In particular, April 30 shows the highest regression coefficient, and if we look at Fig. 3 (top right) we can see good agreement in the retrievals, although the ANN slightly overestimates plume height for values higher than 700 mb. This is reflected in the mean values percentage difference given in the last column of Table 2.

In general, the scatter-plots of Fig. 3 (right-hand column) show a higher spread in plume height than that obtained for the SO_2 total column retrieval (left-hand column). This is confirmed by the regression coefficient obtained and corresponding RMSE. Nevertheless, the ANN estimates show good accuracy with RMSE values lower than corresponding STD for all dates and the percentage difference between the estimate and target means are very low (Table 2, last column).

The regression curves for May 15, depicted in Fig. 3 (middle right and bottom right), show a good performance of the retrieval in the range 500–700 mb (5000–3000 m).

The validation on the Grímsvötn eruption occurring during 2011 May (see description in Section 4.2), was centred on three distinct IASI images for the 2011 May 22, 23 and 24. These images were not considered during the training phase. Statistics for these images are shown in Tables 3 and 4 for SO_2 total amount and plume height, respectively.

In general the SO_2 total column is retrieved with lower accuracy for all three validation dates. Despite regression coefficients similar to those of the Eyjafjallajökull validations, RMSE values are higher. Although this behaviour could be related to a higher distribution's spreading of values as noticed looking at STD values in Table 3,

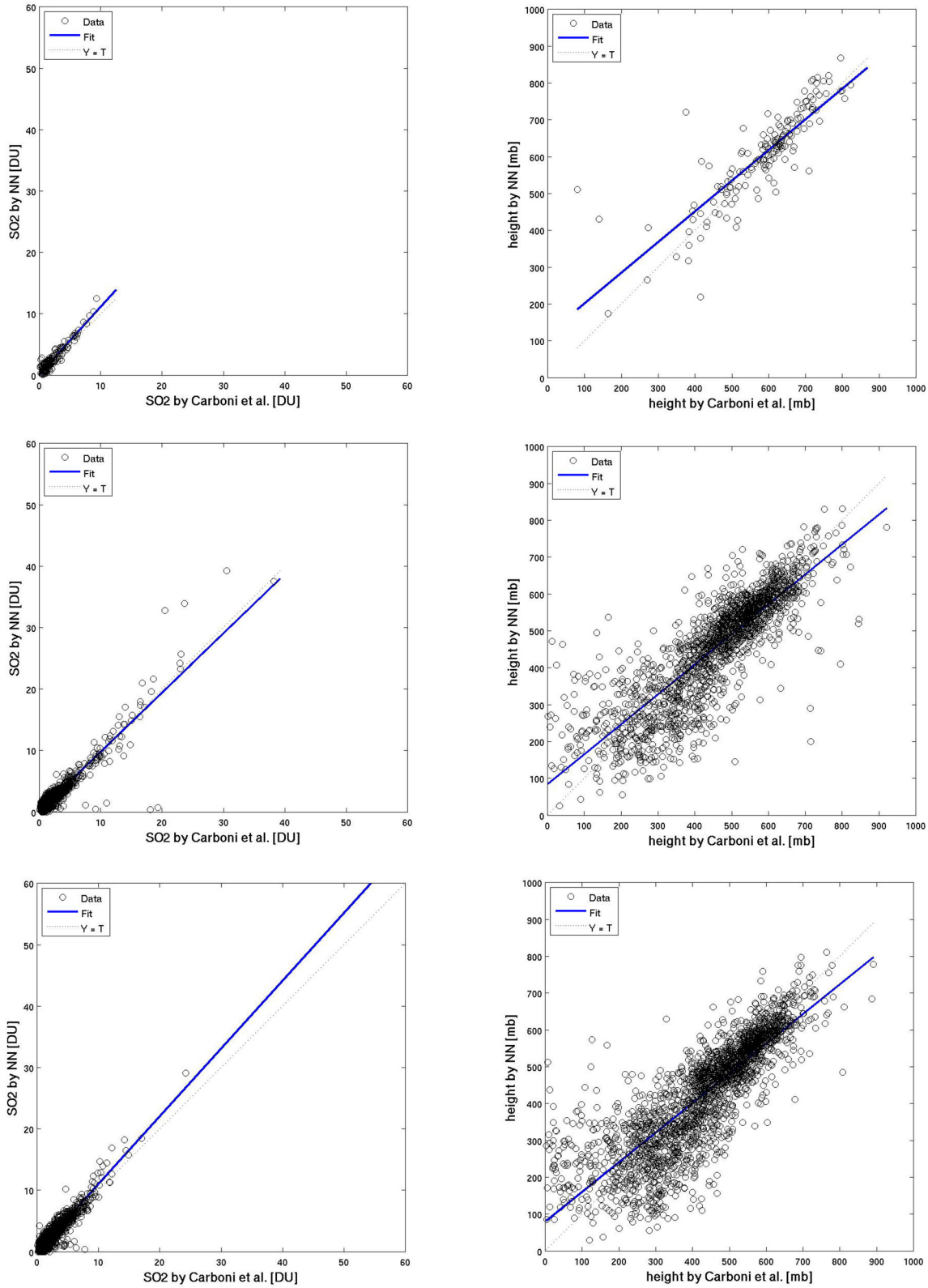

Figure 3. Scatter plots of SO_2 total column amount (left-hand panels) and plume height (right-hand panels) derived from the neural networks method versus the Eyjafjallajökull validation data sets, 2010 April 30, afternoon orbit (top panels), 2010 May 15, morning orbit (middle panels) and 2010 May 15, afternoon orbit (bottom panels).

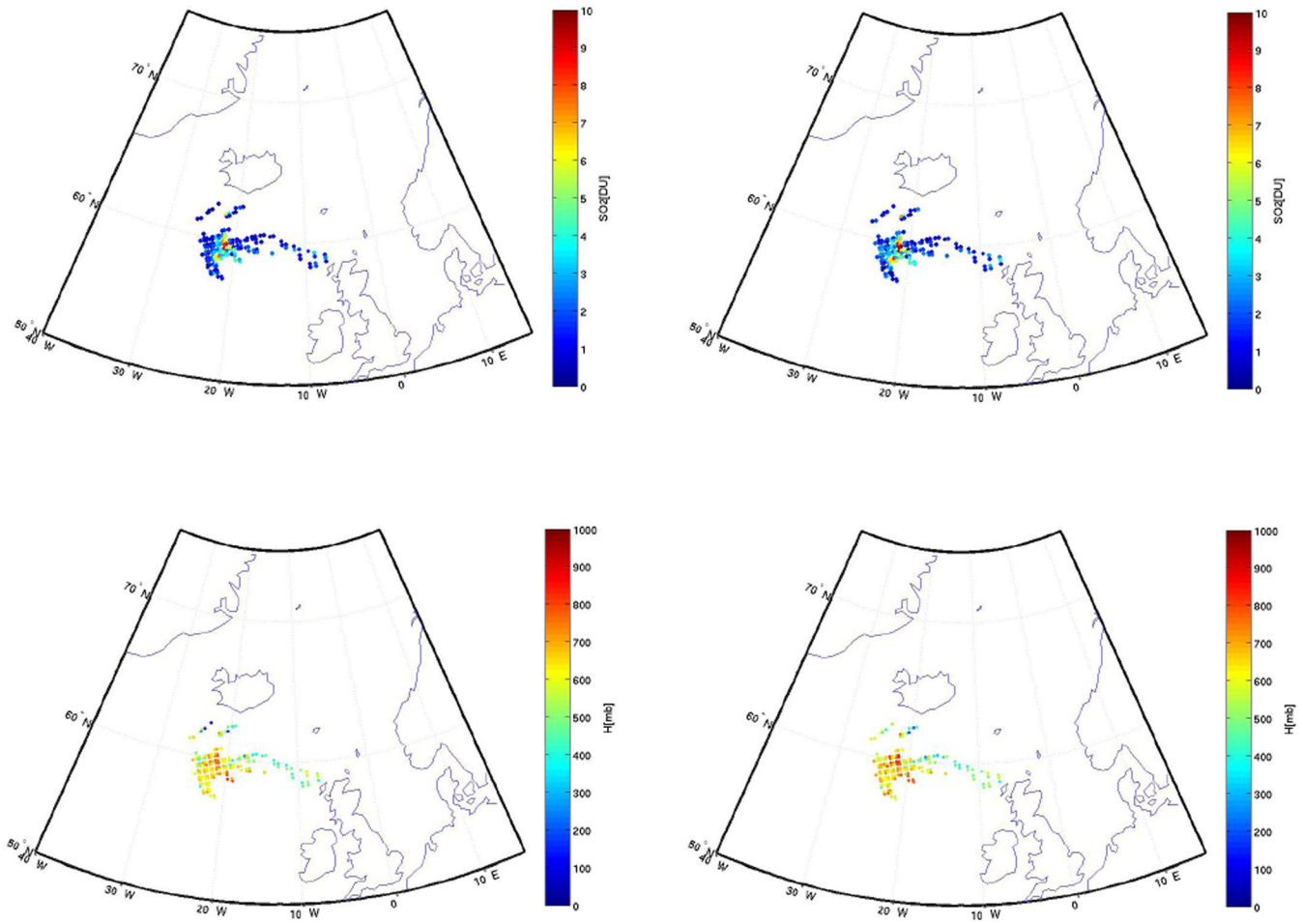

Figure 4. Eyjafjallajökull validation data set, 2010 April 30, afternoon orbit. Top panels: SO_2 total column map from retrieval (left-hand panel) and ANN (right-hand panel). Bottom panels: SO_2 plume height from retrieval (left-hand panel) and ANN (right-hand panel).

looking at the last column in Table 3 we notice that mean difference percentage values are similar to those observed for Eyjafjallajökull, and they reveal that the ANN overestimates SO_2 retrieval in all three cases.

The lower accuracy observed can be analysed in detail using scatter-plots as shown in Fig. 6 (left-hand column) and the maps depicted in Figs 7 and 8 (top). For 2011 May 22, looking at the scatter-plot in Fig. 6 (top-left), we notice how the ANN performance decreases for values higher than 20 DU, revealing an average overestimation of around 1 per cent (Table 3, last column). The behaviour is similar to that observed for Eyjafjallajökull dates, but here a decreasing in accuracy is noticeable for values higher than 20 DU, where overestimation and underestimation is observed.

Similar behaviour is noticeable for the 2011 May 23 estimates in the scatter-plot of Fig. 6 (middle-left). It shows a decreasing of accuracy for SO_2 values higher than 20 DU and mean value difference percentage around 7 per cent, confirming an overestimation again. Also for this date the overestimation and underestimation effect is observed above 20 DU. If we have a look at Fig. 8 (top), the map comparison between target and estimates, we notice the overestimation characterizes pixels on a strip along the 75° N parallel and a portion of the plume lying under Iceland.

A distinct performance is noticed when the ANN is applied to May 24. RMSE is of the order of magnitude of those observed for the Eyjafjallajökull eruption, but the mean difference percentage value is higher, showing a sparse overestimation (Table 4).

This distinct behaviour of performances can be explained by considering that, with the exception of 2011 May 24, the mean values of samples for 2011 are around an order of magnitude greater than those of 2010 Eyjafjallajökull instances, for both training and validation dates.

This loss of accuracy noticed for the Grímsvötn validations, also present with low intensity in the Eyjafjallajökull validations, is an effect caused by a lower statistical representation of such an eruption in training patterns. In fact, values of SO_2 concentration higher than 30 DU represent only 1.5 per cent of training samples (we used only 16 IASI images of the Grímsvötn eruption during the training phase). In other words, the Grímsvötn eruption was characterized by higher SO_2 concentrations statistically not well represented during the training phase.

Table 4 summarizes the results of the ANN to retrieve the Grímsvötn plume height. The May 22 shows the highest RMSE and a slightly higher percentage of retrieval underestimation. Looking at the regression curve in Fig. 6 (top right) we notice a higher spreading phenomenon for values lower than 300 mb with a overestimation/underestimation effect, while ANN underestimates plume height for higher values. Overestimation is noticeable looking at Fig. 7 (top) for those pixels located in the north of Iceland around 70°N, while the core of the plume is well characterized by ANN in height.

The May 23 and 24 test cases have similar values of coefficient regression, around 0.8, and lower values of RMSE (Table 4, column

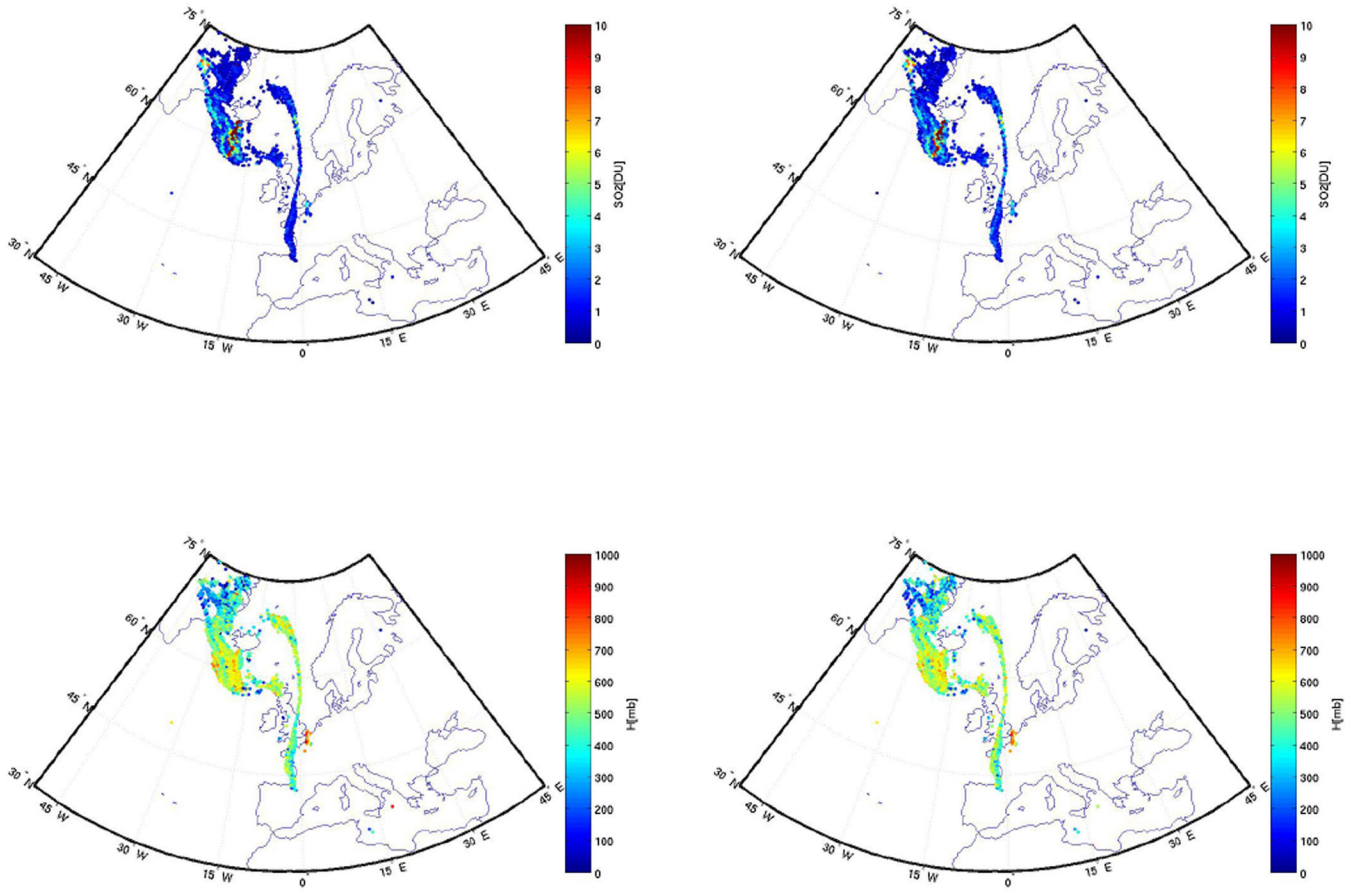

Figure 5. Eyjafjallajökull validation data set, 2010 May 15, morning orbit. Top panels: SO_2 total column map from retrieval (left-hand panel) and ANN (right-hand panel). Bottom panels: SO_2 plume height from retrieval (left-hand panel) and ANN (right-hand panel).

Table 2. Eyjafjallajökull. RMSE and mean percentage difference between the ANN SO_2 plume height and reference retrievals (Carboni *et al.* 2012). Also given are the STD of reference retrievals.

Date	SO_2 plume height				
	N samples	Regr. coeff.	RMSE (mb)	STD (mb)	Mean diff. per cent
2010 April 30 aft	161	0.84749	83.1373	124.5436	3.4880
2010 May 15 mor	1823	0.84314	87.6765	150.8156	−0.4420
2010 May 15 aft	2303	0.83194	71.2645	153.2738	−1.1068

Table 3. Grímsvötn. RMSE and mean percentage difference between the ANN SO_2 total column amount and reference retrievals (Carboni *et al.* 2012). Also given are the STD of reference retrievals.

Date	SO_2 total column				
	N samples	Regr. coeff.	RMSE (DU)	STD (DU)	Mean diff. per cent
2011 May 22	293	0.95702	9.1156	31.3802	1.0412
2011 May 23	678	0.93527	8.3893	22.4618	7.7324
2011 May 24	584	0.97378	1.0346	3.3554	34.5325

Table 4. Grímsvötn. RMSE and mean percentage difference between the ANN SO_2 plume height and reference retrievals (Carboni *et al.* 2012). Also given are the STD of reference retrievals.

Date	SO_2 plume height				
	N samples	Regr. coeff.	RMSE (mb)	STD (mb)	Mean diff. per cent
2011 May 21	293	0.84003	96.6539	178.3696	−0.5960
2011 May 23	678	0.86151	92.3708	177.9770	5.2399
2011 May 24	584	0.82592	95.8029	166.8963	4.2937

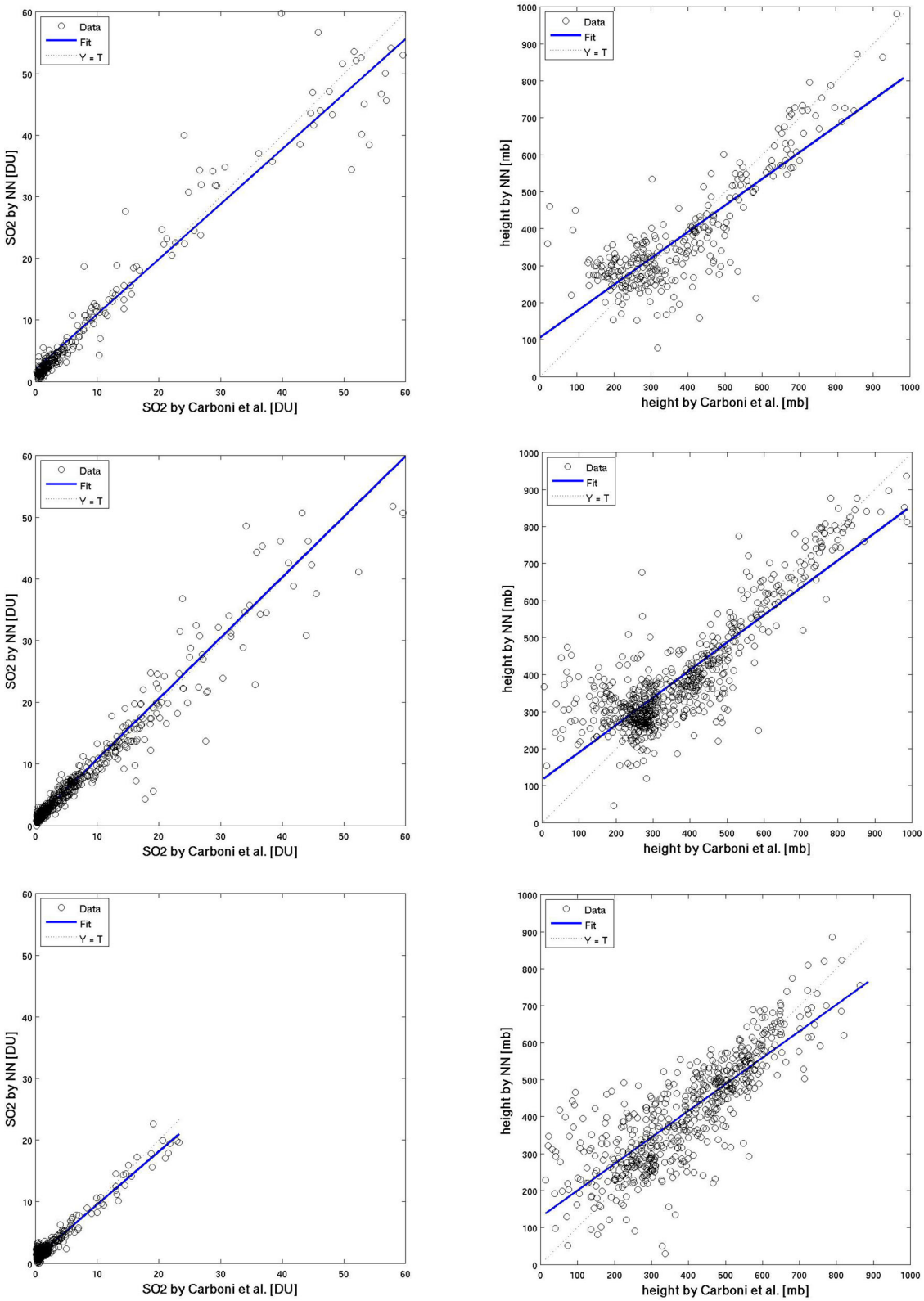

Figure 6. Scatter plots of SO_2 total column amount (left-hand panels) and plume height (right-hand panels) derived from the neural networks method versus the Grímsvötn validation data sets, 2011 May 22 20:00 UTC (top panels), 2011 May 23, 10:00 UTC (middle panels) and 2011 May 24, 18:00 UTC (bottom panels).

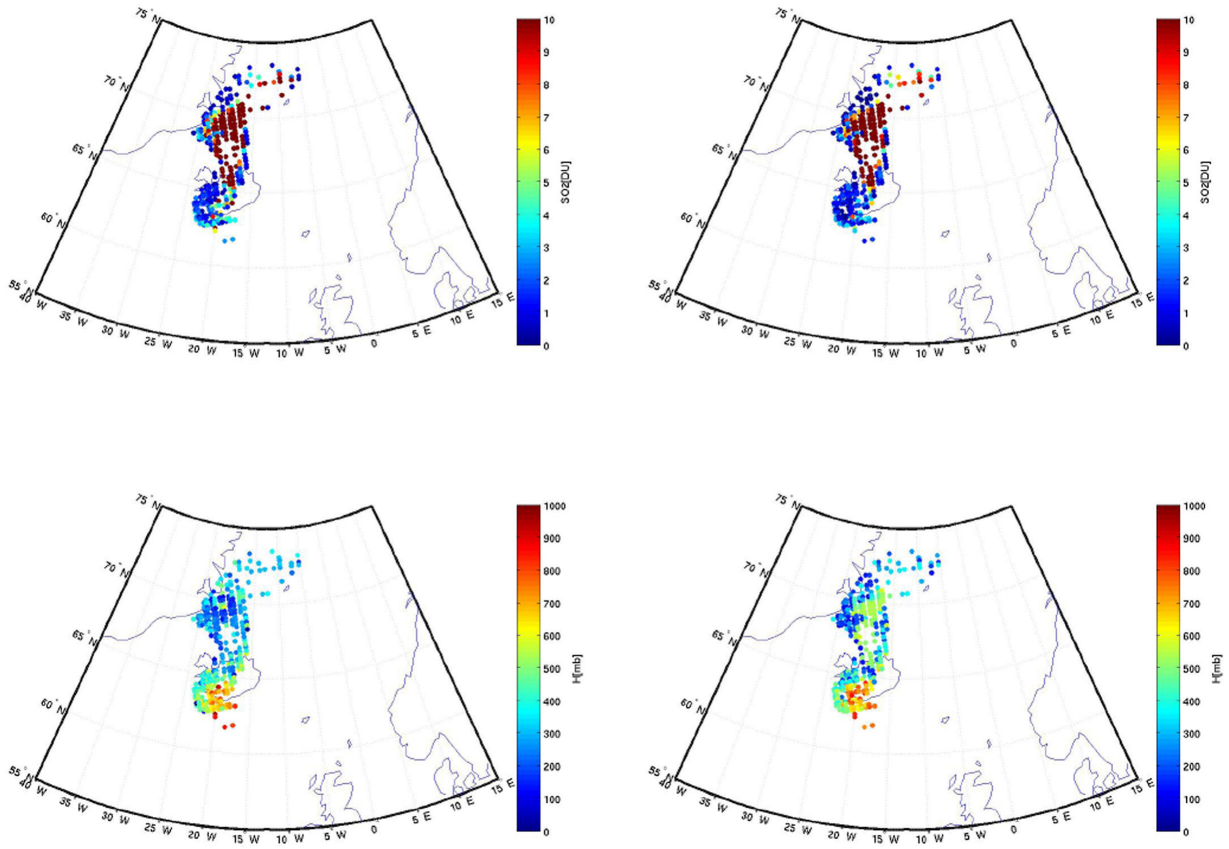

Figure 7. Grímsvötn validation data set, 2011 May 22, 20:00 UTC. Top panels: SO_2 total column amount map from retrieval (left-hand panel) and from ANN (right-hand panel). Bottom panels: SO_2 plume height from retrieval (left-hand panel) and ANN (right-hand panel).

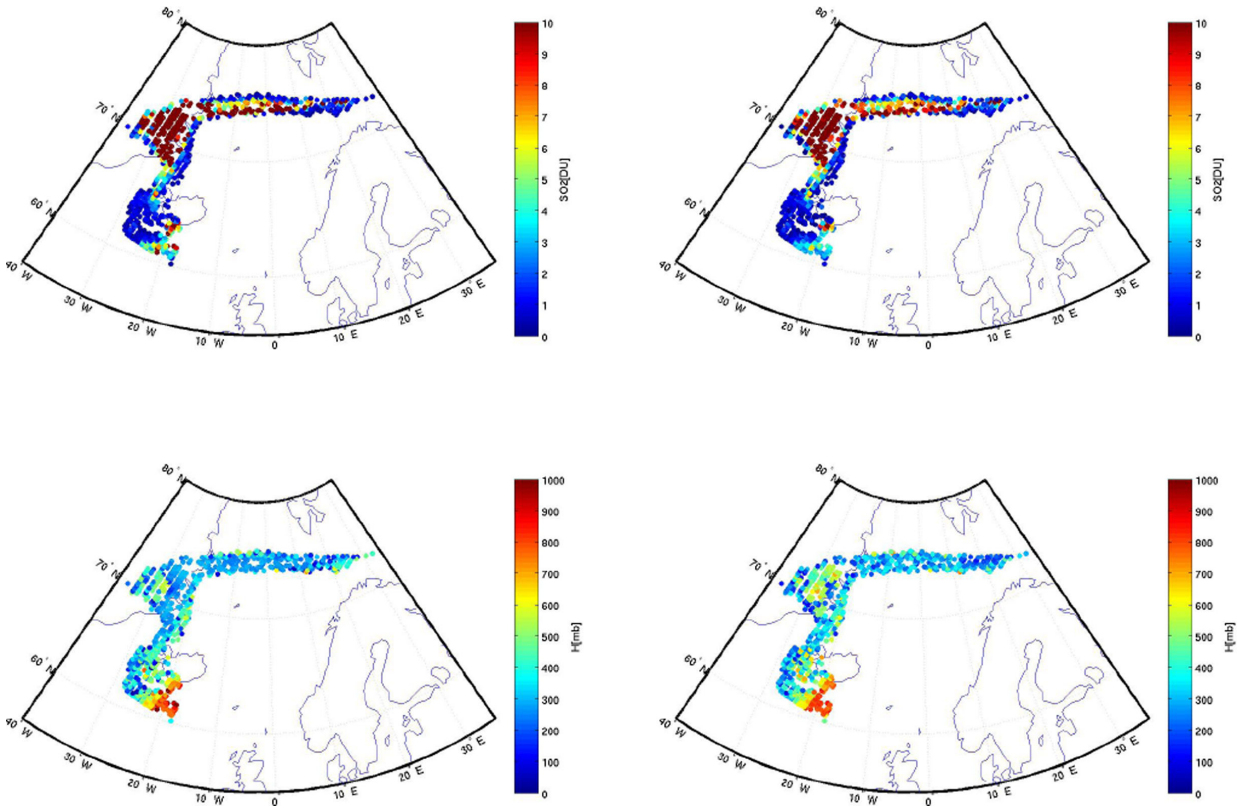

Figure 8. Grímsvötn validation data set, 2011 May 23, 10:00 UTC. Top panels: SO_2 total column amount map from retrieval (left-hand panel) and from ANN (right-hand panel). Bottom panels: SO_2 plume height from retrieval (left-hand panel) and ANN (right-hand panel).

four), and scatter-plots depicted in Fig. 6 (middle-right and bottom-right, respectively), show that the ANN plume height retrieval is overestimated. For May 23, overestimation is located in Greenland, along 70°N (Fig. 8, bottom). In general, looking at the scatter-plots depicted in Fig. 6 (right column) it seems that for plume height estimation the ANN reveals a lower performance than that obtained for SO_2 concentrations.

In the case of plume height estimates, the accuracy decreasing for high values is not present because the Carboni *et al.* (2012) retrievals related to the Grímsvötn eruption are statistically well represented by training data sets, and a lower accuracy is present for those values not well known by ANN during the training phase, for example, around 200 mb (only 6 per cent). In fact, the Grímsvötn eruption revealed higher plume altitudes than the Eyjafjallajökull eruption (see Section 4.2).

6 CONCLUSIONS

This work shows that neural networks can be used to rapidly retrieve SO_2 column amount and altitude from IASI images. ANNs retrieved SO_2 concentrations with high accuracy when applied to Eyjafjallajökull independent data sets. It was also shown that applying the ANNs to the eruption of Grímsvötn (whose plume was at different latitudes and heights in different weather conditions), gave satisfactory results for SO_2, but show a decreasing accuracy for values higher than 20 DU, due mainly to a minor statistical characterization of this eruption during the ANN training phase. Thus a wider adoption of neural network methodology for fast retrieval and near real time monitoring is foreseeable, with the only constraint being to maintain and update the ANN during the operating stage.

For plume height estimation the results have a slightly lower accuracy and more investigation is needed to improve the ANN accuracy.

Despite the high number of inputs involved using IASI data, our work has demonstrated that ANNs are able to emulate an inverse model for volcanic SO_2 and plume height estimation but, given high spectral resolution measurement, the enormous quantity of inputs (1242) may limit the ANNs accuracy and generalization capability. Thus future enhancements will include the use of pruning algorithms or non-linear principal component analysis to extract significant information and reduce the number of inputs.

ACKNOWLEDGEMENTS

EC and RGG acknowledge funding from the NERC COMET. The authors would like to thank Joachim Wasserman and Klemen Zaksek whose comments significantly improved the paper.

REFERENCES

Anderson, G.P., Wang, J. & Chetwynd, J.H., 1995. MODTRAN3: an update and recent validation against airborne high resolution interferometer measurements, in *Summaries of the Fifth Annual Jet Propulsion Laboratory Airborne Earth Science Workshop,* Pasadena, CA, 1995 January 23–26, JPL Publication 95-1, Vol. 1, pp. 5–8.

Basheer, I., 2000. Selection of methodology for modeling hysteresis behavior of soils using neural networks, *Comput-aided Civil Infrastruct. Eng.,* **5**(6), 445–463.

Berk, A., Bernstein, L.S. & Robertson, D.C., 1989. MODTRAN: a moderate resolution model for LOWTRAN 7, GL-TR-89-0122, Spectral Sciences Inc., Burlington, MA.

Bishop, C., 1995. *Neural Networks For Pattern Recognition,* Oxford Univ. Press.

Blackwell, W.J., 2005. A neural-network technique for the retrieval of atmospheric temperature and moisture profiles from high spectral resolution sounding data, *IEEE Trans. Geosci. Remote Sens.,* **43,** 2535–2546.

Blumstein, D. *et al.*, 2004. IASI Instrument: Technical overview and measured performances, *Proc. SPIE,* **5543,** 196–207.

Boynard, A. *et al.*, 2014. First simultaneous space measurements of atmospheric pollutants in the boundary layer from IASI: a case study in the North China Plain, *Geophys. Res. Lett.,* **41**(2), 645–651.

Campion, R. *et al.*, 2010. Measuring volcanic degassing of SO_2 in the lower troposphere with ASTER band ratios, *J. Volc. Geotherm. Res.,* **194,** 42–54.

Carn, S.A., Strow, L.L., de Souza-Machado, S., Edmonds, Y. & Hannon, S., 2005. Quantifying tropospheric volcanic emissions with AIRS: the 2002 eruption of Mt. Etna (Italy), *Geophys. Res. Lett.,* **32,** L02301, doi:10.1029/2004GL021034.

Carboni, E., Grainger, R., Walker, J., Dudhia, A. & Siddans, R., 2012. A new scheme for sulphur dioxide retrieval from IASI measurements: application to the Eyjafjallajökull eruption of April and May 2010, *Atmos. Chem. Phys.,* **12,** 11 417–11 434.

Clarisse, L., Coheur, P.F., Prata, A. J., Hurtmans, D., Razavi, A., Phulpin, T., Hadji-Lazaro, J. & Clerbaux, C., 2008. Tracking and quantifying volcanic SO_2 with IASI, the September 2007 eruption at Jebel at Tair, *Atmos. Chem. Phys.,* **8,** 7723–7734.

Clarisse, L., Hurtmans, D., Clerbaux, C., Hadji-Lazaro, J., Ngadi, Y. & Coheur, P.-F., 2012. Retrieval of sulphur dioxide from the infrared atmospheric sounding interferometer (IASI), *Atmos. Measure. Techniq.,* **5,** 581–594.

Clarisse, L., Coheur, P.-F., Theys, N., Hurtmans, D. & Clerbaux, C., 2014. The 2011 Nabro eruption, a SO_2 plume height analysis using IASI measurements, *Atmos. Chem. Phys.,* **14,** 3095–3111.

Clerbaux, C. *et al.*, 2008. Measurements of SO_2 profiles in volcanic plumes from the NASA Tropospheric Emission Spectrometer (TES), *Geophys. Res. Lett.,* **35,** L22807, doi:10.1029/2008GL035566.

Clerbaux, C. *et al.*, 2009. Monitoring of atmospheric composition using the thermal infrared IASI/MetOp sounder, *Atmos. Chem. Phys.,* **9,** 6041–6054.

Corradini, S., Spinetti, C., Carboni, E., Tirelli, C., Buongiorno, M.F., Pugnaghi, S. & Gangale, G., 2008. Mt. Etna tropospheric ash retrieval and sensitivity analysis using Moderate Resolution Imaging Spectroradiometer measurements, *J. appl. Remote Sens.,* **2**(1), 023550, doi:10.1117/1.3046674.

Corradini, S., Merucci, L. & Prata, A.J., 2009. Retrieval of SO_2 from thermal infrared satellite measurements: correction procedures for the effects of volcanic ash, *Atmos. Measur. Techniq. Discuss.,* **2,** 303–342.

Corradini, S., Merucci, L., Prata, A.J. & Piscini, A., 2010. Volcanic ash and SO_2 in the 2008 Kasatochi eruption: Retrievals comparison from different IR satellite sensors, *J. geophys. Res.,* **115,** D00L21, doi:10.1029/2009JD013634.

Del Frate, F., Ortenzi, A., Casadio, S. & Zehner, C., 2002. Application of neural algorithms for a real-time estimation of ozone profiles from GOME measurements, *IEEE Trans. Geosci. Remote Sens.,* **40,** 2263–2270.

Faure, T., Isaka, H. & Guillemet, B., 2002. Neural network retrieval of cloud parameters from high-resolution multispectral radiometric data: A feasibility study, *Remote Sens. Environ.,* **80**(2), 285–296.

Gardner, M.W. & Dorling, S.R., 1998. Artificial neural networks (the multilayer perceptron) – A review of applications in the atmospheric sciences, *Atmos. Environ.,* **32,** 2627–2636.

Geman, S., Bienenstock, E. & Doursat, R., 1992. Neural networks and the bias variance dilemma, *Neural Comput.,* **4**(1), 1–58.

Hassoun, M.H., 1995. *Fundamentals of Artificial Neural Networks,* MIT Press.

Haykin, S. (1999). *Neural Networks A Comprehensive Foundation,* 2nd edn, Prentice-Hall.

Hecht-Nielsen, R., 1990. *Neurocomputing,* Addison-Wesley.

Hsieh, W.W. & Tang, B., 1998. Applying neural network models to prediction and data analysis in meteorology and oceanography, *Bull. Am. Meteorol. Soc.,* **79,** 1855–1870.

Krotkov, N.A., Carn, S.A., Krueger, A.J., Bhartia, P.K. & Yang, K., 2006. Band residual difference algorithm for retrieval of SO2 from the Aura Ozone Monitoring Instrument (OMI), *IEEE Trans. Geosci. Remote Sens.,* **44,** 1259–1266.

Lek, S. & Guegan, J.F., 1999. Artificial neural networks as a tool in ecological modelling, an introduction, *Ecol. Model.,* **120,** 65–73.

Marzano, F.S., Lamantea, M., Montopoli, M., Di Fabio, S. & Picciotti, E., 2011. The Eyjafjoll explosive volcanic eruption from a microwave weather radar perspective, *Atmos. Chem. Phys.,* **11,** 9503–9518.

Masters, T., 1994. *Practical Neural Network Recipes in C++,* Academic Press.

Miller, T.P. & Casadevall, T.J., 2000. Volcanic ash hazards to aviation, in *Encyclopedia of Volcanoes,* pp. 915–930, ed. Sigurdsson, H., Academic Press, San Diego, CA, USA.

Nowlan, C.R., Liu, X., Chance, K., Cai, Z., Kurosu, T.P., Lee, C. & Martin, R.V., 2011. Retrievals of sulfur dioxide from the Global Ozone Monitoring Experiment 2 (GOME-2) using an optimal estimation approach: algorithm and initial validation, *J. geophys. Res.,* **116,** D18301, doi:10.1029/2011JD015808.

Picchiani, M., Chini, M., Corradini, S., Merucci, L., Sellitto, P., Del Frate, F. & Stramondo, S., 2011. Volcanic ash detection and retrievals using MODIS data by means of neural networks, *Atmos. Measur. Techniq.,* **4,** 2619–2631.

Piscini, A., Picchiani, M., Chini, M., Corradini, S., Merucci, L., Del Frate, F. & Stramondo, S., 2014. A neural network approach for the simultaneous retrieval of volcanic ash parameters and SO_2 using MODIS data, *Atmos. Meas. Tech. Discuss.,* **7,** 3349–3395.

Prata, A.J. & Bernardo, C., 2007. Retrieval of volcanic SO_2 column abundance from Atmospheric Infrared Sounder data, *J. geophys. Res.,* **112,** D20204, doi:10.1029/2006JD007955.

Prata, A.J. & Kerkmann, J., 2007. Simultaneous retrieval of volcanic ash and SO_2 using MSG-SEVIRI measurements, *Geophys. Res. Lett.,* **34,** L05813, doi:10.1029/2006GL028691.

Prechelt, L., 1998. Automatic early stopping using cross validation: quantifying the criteria, *Neural Networks,* **11**(4), 761–767.

Pugnaghi, S., Gangale, G., Corradini, S. & Buongiorno, M.F., 2006. Mt. Etna sulfur dioxide flux monitoring using ASTER-TIR data and atmospheric observations, *J. Volc. Geotherm. Res.,* **152,** 74–90.

Realmuto, V.J., 2000. The potential use of Earth Observing System data to monitor the passive emission of sulfur dioxide from volcanoes, *Geoph. Monog. Series,* **116,** 101–115.

Realmuto, V.J., Sutton, A.J. & Elias, T., 1997. Multispectral thermal infrared mapping of sulfur dioxide plumes: A case study from the East Rift Zone of Kilauea Volcano, Hawaii, *J. geophys. Res.,* **102,** 15 057–15 072.

Realmuto, V.J., Berk, A., Acharya, P.K. & Kennett, R., 2013. Advances in the validation of Satellite-Based Maps of Volcanic Sulfur Dioxide Plumes, *Presented at AGU Fall 2013 Meeting,* San Francisco, 2013 December 9–12.

Rix, M. *et al.*, 2012. Volcanic SO_2, BrO and plume height estimations using GOME-2 satellite measurements during the eruption of Eyjafjallajökull in May 2010, *J. geophys. Res.,* **117,** D00U19, doi:10.1029/2011JD016718.

Rodgers, C.D., 2000. *Inverse Methods for Atmospheric Sounding: Theory and Practice,* World Scientific.

Rumelhart, D.E., Hinton, G.E. & Williams, R.J., 1986. Learning internal representation by error propagation, in *Parallel Distributed Processing: Exploration in the Microstructure of Cognition,* Chapter 8, Vol. 1, pp. 318–362, eds Rumelhart, D.E. & McClleland, J.L., MIT Press.

Rumelhart, D.E., Durbin, R., Golden, R. & Chauvin, Y., 1995. Backpropagation: the basic theory, in *Backpropagation: Theory, Architecture, and Applications,* pp. 1–34, eds Rumelhart, D.E. & Yves, C., Lawrence Erlbaum.

Saunders, R.W., Matricardi, M. & Brunel, P., 1999. An improved fast radiative transfer model for assimilation of satellite radiance observations, *Q. J. Roy. Meteor. Soc.,* **125,** 1407–1425.

Schlüssel, P., Hultberg, T.H., Phillips, P.L., August, T. & Calbet, X., 2005. The operational IASI level 2 processor, *Adv. Space Res.,* **36,** 982–988.

Smithsonian Institution, Global Volcanism Program. Available at: http://www.volcano.si.edu,10.1093/gji/ggu152.html (last accessed June 2013).

Stohl, A. *et al.*, 2011. Airborne observations of the Eyjafjalla volcano ash cloud over Europe during air space closure in April and May 2010, *Atmos. Chem. Phys.,* **11,** 2245–2279.

Thomas, H.E. & Prata, A.J., 2011. Sulphur dioxide as a volcanic ash proxy during the April–May 2010 eruption of Eyjafjallajökull Volcano, Iceland, *Atmos. Chem. Phys.,* **11,** 6871–6880.

Urai, M., 2004. Sulfur dioxide flux estimation from volcanoes using advanced spaceborne thermal emission and reflection radiometer: a case study of Miyakejima volcano, Japan, *J. Volc. Geotherm. Res.,* **134,** 1–13.

Vasudevan, B.G., Gohil, B.S. & Agarwal, V.K., 2004. Backpropagation neural-network-based retrieval of atmospheric water vapor and cloud liquid water from IRS-P4 MSMR, *IEEE Trans. Geosci. Remote Sens.,* **42,** 985–990.

Walker, J.C., Dudhia, A. & Carboni, E., 2011. An effective method for the detection of trace species demonstrated using the MetOp Infrared Atmospheric Sounding Interferometer, *Atmos. Measur. Techniq.,* **4,** 1567–1580.

Walker, J.C., Carboni, E., Dudhia, A. & Grainger, R.G., 2012. Improved detection of sulphur dioxide in volcanic plumes using satellite-based hyperspectral infra-red measurements: application to the Eyjafjallajökull 2010 eruption, *J. geophys. Res.,* **117,** D00U16, doi:10.1029/2011JD016810.

Watson, I.M., Realmuto, V.J., Rose, W.I., Prata, A.J., Bluth, G.J.S., Gu, Y., Bader, C.E. & Yu, T., 2004. Thermal infrared remote sensing of volcanic emissions using the moderate resolution imaging spectroradiometer, *J. Volc. Geotherm. Res.,* **135**(1–2), 75–89.

Yang, K., Liu, X., Krotkov, N.A., Krueger, A.J. & Carn, S.A., 2009. Estimating the altitude of volcanic sulfur dioxide plumes from space borne hyper-spectral UV measurements, *Geophys. Res. Lett.,* **36,** L10803, doi:10.1029/2009GL038025.

Zehner, C., ed., 2010. Monitoring volcanic ash from space, in *Proceedings of the ESA-EUMETSAT Workshop on the 14 April to 23 May 2010 Eruption at the Eyjafjoll Volcano,* South Iceland. Frascati, Italy, 2010 May 26–27, ESA-Publication STM-280, doi:10.5270/atmch-10-01.